AGU PUBLICATIONS

JGR

Journal of Geophysical Research: Oceans

RESEARCH ARTICLE

10.1002/2016JC012494

Submesoscale processes promote seasonal restratification in the Subantarctic Ocean

M. du Plessis[1,2], S. Swart[1,2,3], I. J. Ansorge[1], and A. Mahadevan[4]

[1]Department of Oceanography, Marine Research Institute, University of Cape Town, Rondebosch, South Africa, [2]Southern Ocean Carbon and Climate Observatory, CSIR, Stellenbosch, South Africa, [3]Now at Department of Marine Sciences, University of Gothenburg, Gothenburg, Sweden, [4]Physical Oceanography Department, Woods Hole Oceanographic Institution, Woods Hole, Massachusetts, USA

Key Points:
- Seasonal restratification defined using ocean glider observations cannot be explained by seasonal warming alone
- Up-front winds and increased ML horizontal buoyancy gradients promote restratification by submesoscale ML eddies in spring
- Fluxes of wind-driven Ekman buoyancy flux at horizontal buoyancy fronts compete with restratifying ML eddies to mix the upper ocean

Correspondence to:
M. du Plessis,
dplmar020@myuct.ac.za

Citation:
du Plessis, M., S. Swart, I. J. Ansorge, and A. Mahadevan (2017), Submesoscale processes promote seasonal restratification in the Subantarctic Ocean, *J. Geophys. Res. Oceans*, *122*, 2960–2975, doi:10.1002/2016JC012494.

Received 21 OCT 2016
Accepted 8 MAR 2017
Accepted article online 14 MAR 2017
Published online 8 APR 2017

Abstract Traditionally, the mechanism driving the seasonal restratification of the Southern Ocean mixed layer (ML) is thought to be the onset of springtime warming. Recent developments in numerical modeling and North Atlantic observations have shown that submesoscale ML eddies (MLE) can drive a restratifying flux to shoal the deep winter ML prior to solar heating at high latitudes. The impact of submesoscale processes on the intraseasonal variability of the Subantarctic ML is still relatively unknown. We compare 5 months of glider data in the Subantarctic Zone to simulations of a 1-D mixing model to show that the magnitude of restratification of the ML cannot be explained by heat, freshwater, and momentum fluxes alone. During early spring, we estimate that periodic increases in the vertical buoyancy flux by MLEs caused small increases in stratification, despite predominantly down-front winds that promote the destruction of stratification. The timing of seasonal restratification was consistent between 1-D model estimates and the observations. However, during up-front winds, the strength of springtime stratification increased over twofold compared to the 1-D model, with a rapid shoaling of the MLD from >200 m to <100 m within a few days. The ML stratification is further modified under a negative Ekman buoyancy flux during down-front winds, resulting in the destruction of ML stratification and deepening of the MLD. These results propose the importance of submesoscale buoyancy fluxes enhancing seasonal restratification and mixing of the Subantarctic ML.

1. Introduction

1.1. Subantarctic Mixed Layer

This work follows the seasonal restratification of Subantarctic mixed layer (ML). Classical thinking depicts that summertime restratification within the Subantarctic Zone (SAZ) is driven by the onset of warming, restratifying deep winter mixed layer depths (MLDs), which often extend over 400 m [*Sallée et al*., 2010] to shallower than 100 m during summer [*Rintoul and Trull*, 2001; *Swart et al*., 2015]. A fundamental implication of the seasonal restratification is the extended availability of light to phytoplankton, which photosynthetically fix carbon at globally important rates. The Southern Ocean alone contributes to about one-third of the global organic carbon flux [*Schlitzer*, 2002], making seasonal variations of the ML an important component of the global carbon system. However, climate models are unable to accurately represent Southern Ocean ML [*Sallée et al*., 2013]. Furthermore, *Thomalla et al*. [2011] indicate clear inconsistencies in the timing of enhanced seasonal phytoplankton growth and heat fluxes. Recently, *Swart et al*. [2015] use a high-resolution glider data set to show that spring and summer MLD variations can be separated into two distinct regimes. The springtime MLD undergoes large vertical migrations between the surface and the deep seasonal pycnocline (200–300 m), while during summer the MLD is consistently bound to a shallower (<100 m) seasonal pycnocline. Importantly, they show that during spring, periodic restratification events occur in the presence of horizontal density gradients, suggesting that seasonal variations of stratification in the SAZ are not solely driven by air-sea fluxes as these restratification events occur too rapidly to be attributed to surface heating alone. *Swart et al*. [2015] also reveal that spring restratification is concurrent with enhanced primary production, while *Thomalla et al*. [2015] apply the same data set to show this bloom initiation to be associated with increased light availability due to these periods of enhanced restratification. Both studies allude the spring restratification and bloom initiation to submesoscale processes based on

numerical model studies and Northern Hemisphere observations. This study aims to elucidate the role of submesoscale processes during seasonal restratification of the SAZ ML, which is particularly important in the context of coupled physical-biological dynamics, and therefore for climate.

1.2. Restratification by Submesoscale Mixed Layer Eddies (MLE)

Developments in numerical modeling have greatly enhanced our understanding of ocean processes occurring at the submesoscale [*Haine and Marshall*, 1998; *Thomas and Lee*, 2005; *Boccaletti et al*., 2007; *Fox-Kemper et al*., 2008; *Mahadevan et al*., 2010]. Submesoscale flows develop in localized regions of the surface ocean where the vertical component of the relative vorticity attains a magnitude as large or larger than the planetary vorticity. These often occur due to mesoscale straining and frontogenic processes which lead to an intensification of the frontal jet due to enhanced thermal wind shear. Submesoscale flows develop within horizontal scales of the ML deformation radius (typically around 10 km) [*Hosegood et al*., 2006] where the flow is no longer influenced by the Earth's rotation.

Frontally geostrophic flow with weak stratification can spontaneously become baroclinically unstable [*Boccaletti et al*., 2007] and lead to the formation of ML eddies (MLEs). MLEs apply a thermally direct overturning circulation within the ML that draws on the potential energy stored in the upright front. MLEs move the lighter water of the front up and over the heavier water to tilt isopycnals toward the horizontal, restratifying the ML. MLEs are difficult to observe due to their small spatial (0.1–10 km) and rapidly evolving (few days) scales. However, owing to their ability to observe the ocean at high space and temporal resolutions, ocean gliders are beginning to reveal the role of MLEs on the restratification of the ocean ML [*Mahadevan et al*., 2012; *Swart et al*., 2015; *Thompson et al*., 2016]. *Mahadevan et al*. [2012] provide observational evidence of MLE processes driving a springtime restratification of the ML affecting the timing of the North Atlantic seasonal phytoplankton bloom initiation. *Thompson et al*. [2016] show a distinct seasonal cycle in ML instabilities and highlight the role MLEs have on periodic restratification during the boreal winter. Both studies are North Atlantic focused, while the Southern Ocean has received limited consideration. However, Southern Ocean focused models are beginning to suggest that submesoscale processes may be important in upper ocean dynamics [*Nikurashin et al*., 2013; *Rosso et al*., 2014; *Forryan et al*., 2015]. Additionally, a study by *Monteiro et al*. [2015] use hourly observations of CO_2 fluxes in the SAZ to indicate the necessity of subdaily sampling to resolve intraseasonal upper ocean dynamics which have potentially important biogeochemistry related variability. These results place important emphasis on the need for ocean observations at the right space and time scales in the Southern Ocean.

1.3. The Impact of Winds on MLEs

Work done by wind on the stratification [*Thomas and Ferrari*, 2008; *Thomas and Taylor*, 2010; *Mahadevan et al*., 2010] has shown that winds aligned with the geostrophic current inputs energy into the upper ocean and drives a horizontal Ekman advection across the front. *Mahadevan et al*. [2010] examined MLE-driven restratification in the presence of winds. They show when the direction of the wind is down stream of the frontal current (down-front), and is sufficiently strong, a surface Ekman flow occurs from the dense side of the front to the light side, keeping the isopycnals of the front upright and preventing MLEs from restratifying the ML. *D'Asaro et al*. [2011] use observations at a front in the Kuroshio Current to show that down-front winds impart an Ekman buoyancy flux (EBF) to catalyze a release of energy in the front, enhancing the turbulence by one to two orders of magnitude. They postulate these processes to be important in regions such as the Antarctic Circumpolar Current (ACC). However, should the wind direction be reversed, it will effectively hasten the restratification process by driving a flow of lighter water over the heavier side of the front. We postulate that the role of the intense westerly winds of the Southern Ocean may be important in opposing any ML restratification flux imposed by MLEs.

1.4. Focus of This Study

Following *Swart et al*. [2015] and *Thomalla et al*. [2015], the deployment of an autonomous ocean glider during the Southern Ocean Seasonal Cycle Experiment (SOSCEx) [*Swart et al*., 2012] is used to study the seasonal restratification in the SAZ. This study presents almost 5 months of continuous, in situ water column observations from the early austral spring in 2012 to the late summer of 2013 (Figure 1). This paper aims to provide more detail of the observed submesoscale field of the SAZ and characterize the role of horizontal buoyancy gradients and MLEs in setting the ML restratification observed in *Swart et al*. [2015]. We use a 1-D vertical mixing model to separate the stratification driven by air-sea heat and momentum fluxes from the

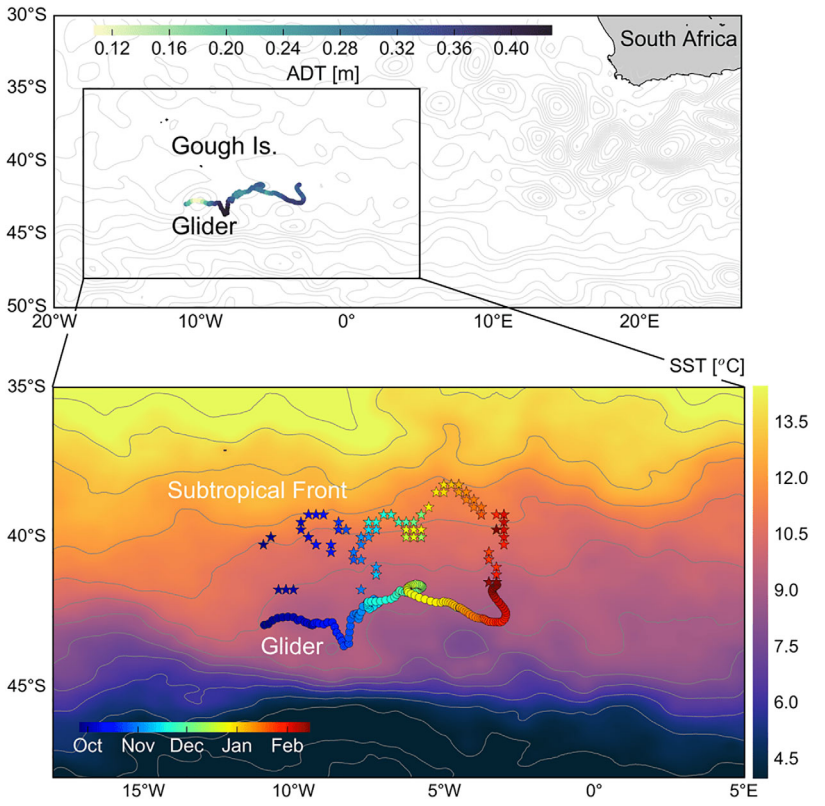

Figure 1. (top) The trajectory covered by the Seaglider (SG573) for the duration of our field campaign SOSCEx (25 September 2012 to 15 February 2013). Colors represent the Absolute Dynamic Topography (ADT) value at each daily mean glider dive location acquired from the AVISO product. The backdrop represents the ADT contours of the day of deployment separated by 0.1 dyn m. (bottom) Circles show the SG573 transect, while the stars show the location of the Subtropical Front. Both are colored to represent the date of each respective daily location, so that the date of the SG573 dive and the location of the Subtropical front are comparable. Background color indicates the SST from the OSTIA product for the date of deployment. Contours of SST are colored gray and separated by 1°C.

glider observed ocean stratification. Following this, we compare the restratifying flux by MLEs, the wind-driven EBF and the surface heat fluxes of the region. In summary, we characterize the processes that set the seasonal stratification in the SAZ and provide unique observational evidence of submesoscale flows in the open Southern Ocean.

2. Data and Methods

2.1. Glider Sampling Strategy

Ocean gliders have proven to be efficient platforms in acquiring high spatial and temporal ML variability [e.g., *Ruiz et al*., 2009]. The glider used in this work (Seaglider 573) continuously sampled in a "V-shaped" pattern from the surface to a nominal depth of 1000 m and back to the surface. The horizontal and temporal resolution of a given dive is dependent on the slope of the V-shape pattern, where during this experiment, an average horizontal resolution of 1.4 $\pm$ 0.9 km and an average temporal resolution of 2 h $\pm$ 56 min per profile (two profiles per dive) was obtained. A total of 1164 profiles were obtained with a mean horizontal velocity of 0.3 m s^{-1} and a nominal vertical velocity of 0.1 m s^{-1} for the period. The hydrographic data were obtained using a Sea-Bird Electronics SBE41 unpumped conductivity (salinity), temperature, and depth profiler (CT-Sail), which sampled with an average rate of 0.2 Hz, attaining a vertical resolution of approximately 0.5 m. At the deployment and retrieval of the glider, ship-based CTD casts were completed, together with salinity, dissolved oxygen, and chlorophyll-a bottle collections, in order to calibrate the glider sensors. Salinity measurements were checked and corrected for conductivity sensor drift, while glider salinity accuracy was calculated to be within 0.03 [see *Swart et al*., 2015, for further detail]. SG573 was deployed on 25 September 2012, south of Gough Island in the South Atlantic Ocean (42.9°S, 11°W) and steered predominantly

eastward and remaining within the frontal bounds of the SAZ. The glider was retrieved on 15 February 2013 (41.6°S, 3.2°W), spending a total of 143 days within the SAZ (Figure 1).

2.2. 1-D ML Model

In this paper, we use the Price-Weller-Pinkel (PWP) [*Price et al*., 1986] ML model as a diagnostic tool to separate the effects of 1-D (vertical) processes from other 3-D processes captured in the observations. PWP destratifies the ML through a momentum flux induced by winds, cooling and evaporation, inducing convective instability, entrainment from the pycnocline and a mixing term generated by vertical current shear. PWP restratifies the ML through surface heating and precipitation. The surface heat flux term, Q_{NET}, is composed of the combination shortwave and longwave radiation, as well as latent and sensible heat fluxes where all components are positive into the ocean. Additionally, PWP requires an evaporation minus precipitation (E) term and wind stress (τ). Evaporation is calculated directly from the latent heat flux. Q_{NET} is absorbed into the water column with a double exponential depth dependence. As the best fit to our study site, we use the e-folding penetrative depth of an open ocean water type determined by *Paulson and Simpson* [1977] where red light penetrates to 0.6 m and blue-green light to 20 m.

PWP was initiated with an average of the first 25 glider profiles of T & S and run for the duration of SOSCEx (143 days). Momentum and heat fluxes were applied at 6 h intervals to match the resolution of the satellite products. Identification of the MLD at each time step throughout the PWP run was achieved by the density difference criteria of 0.03 kg m^{-3} from a 10 m reference level [*de Boyer Montégut et al*., 2004]. It is noted within this work that the along-track glider observations may depict a bias due to the effects of advective, submesoscale, or other internal processes. However, the aim of this experiment is to separate the stratification driven by changes in the 1-D environment determined from momentum and heat fluxes from the regional advancement of in situ seasonal stratification. This provides a basis to characterize changes in ML stratification driven by 3-D processes.

2.3. Satellite Products: Local Atmospheric Forcing

2.3.1. Winds and Freshwater Fluxes

Wind and rainfall data were obtained from the National Centers for Environmental Prediction (NCEP) taken at 10 m above sea level reference height and the surface, respectively (http://www.esrl.noaa.gov/psd/data/gridded/data.ncep.reanalysis.pressure.html). The amalgamation produces a 1/4° gridded field at 6 h intervals at UTC/GMT 00, 06, 12, and 18Z. Wind speed was converted to wind stress using the methods from *Large and Pond* [1981].

2.3.2. Heat Fluxes

Due to limited direct observations and a lack of validation studies of solar heat fluxes (Q_{NET}) in the Southern Ocean, applying the most accurate reanalysis Q_{NET} presents challenges. In this work, our choice of Q_{NET} was identified from two-independent studies which performed a correlation analysis between various reanalysis products and in situ measurements within the Southern Ocean [*Caulet et al*., 2015] and Indian Ocean (A. Tandon, personal communication). The Modern-Era Retrospective Analysis for Research and Applications (MERRA) provided stronger correlations in both sites, and is therefore used in this work. MERRA reanalysis is produced using the Goddard Earth Observing System atmospheric model and data assimilation system [*Rienecker et al*., 2011]. Observational inputs into MERRA include those from ship and buoy measurements with satellite radiances from the Geostationary Operational Environmental Satellite sounder, Television and Infrared Observation Satellite, Operational Vertical Sounder, Advanced TOVS instruments, the Atmospheric Infrared Sounder, the Microwave Sounding Unit, the Advanced Microwave Sounding Unit-A, and SSM/I. Further information regarding the system, the input data streams and their sources, and the observation and background error statistics can be found in *Rienecker et al.* [2011].

2.3.3. Sea Surface Temperature

Maps of sea surface temperature (SST) are used to provide regional scale understanding of the physical environment of the glider observations. The SST data set used in this work is produced at 1 km resolution by Jet Propulsion Laboratory Regional Ocean Modelling group uses satellite data from sensors that include Advanced Very High Resolution Radiometer (AVHRR), the Advanced Along Track Scanning Radiometer (AATSR), the Spinning Enhanced Visible and Infrared Imager (SEVIRI), the Advanced Microwave Scanning Radiometer-EOS (AMSRE), the Tropical Rainfall Measuring Mission Microwave Imager (TMI), the Moderate Resolution Imaging Spectroradiometer (MODIS), the Geostationary Operational Environmental Satellite

(GOES) Imager, the Multi-Functional Transport Satellite 1R (MTSAT-1R) radiometer, and in situ data from drifting and moored buoys (http://ourocean.jpl.nasa.gov/SST/#).

2.4. Submesoscale Mixed Layer Dynamics

Fox-Kemper et al. [2008] provide a parameterization of the restratification process by MLEs restratification. *Mahadevan et al*. [2012] showed this parameterization could be represented in terms of a equivalent restratifying heat flux by MLEs comparable to surface heat fluxes (Q_{MLE}, equation (1)). The application of Q_{MLE} is consistent with analysis provided in the Northern Hemisphere studies [*Mahadevan et al*., 2012; *Thompson et al*., 2016]. As MLEs convert horizontal buoyancy gradients to vertical stratification, Q_{MLE} is dependent on the strength of the horizontal buoyancy gradients and the MLD,

$$Q_{MLE} = C_e \frac{b_y^2 H^2}{f} \frac{C_p \rho}{\alpha g} \mu(z), \tag{1}$$

where is f the Coriolis parameter, C_p the specific heat capacity of seawater, α the thermal expansion coefficient of seawater, g the gravitational acceleration, ρ is the density, b_y is the horizontal buoyancy gradient sampled by the glider, and H is the MLD. C_e is an empirically defined coefficient determined by numerical models [*Fox-Kemper et al*., 2008] and taken to be 0.06. We accept this may not be a true representation of the Southern Ocean but is currently our best estimate available. It should be noted that the strength of the restratification process is not uniform throughout the ML, rather it reaches a maximum at the center of the ML and decreases toward zero at the surface and MLD [*Fox-Kemper et al*., 2008]. The vertical structure function $\mu(z)$ defines this relative rate of restratification for Q_{MLE} at the various depths within the ML. For simplicity, we set $\mu(z)$ to 1 to represent the maximum restratification occurring within the ML for each buoyancy flux parameterization.

Winds directed along the flow of the front will oppose MLE through an Ekman transfer of water from the dense side of the front over the lighter side. Therefore, this wind-driven mechanism reduces ocean stratification where the wind stress is aligned with the geostrophic shear [*Thomas*, 2005]. For Q_{MLE}, an equivalent heat flux for the wind-driven EBF can be expressed as,

$$Q_{Ekman} = \frac{b_y \tau^x}{f} \frac{C_p}{\alpha g}, \tag{2}$$

with τ^x the down-front component of the wind stress. The strength of the horizontal buoyancy gradients and the down-front wind stress are the two important varying factors that drive the strength of the wind-driven flux. The zonal orientation of the mean fronts of the ACC (Figure 1) is aligned with the westerly component of the wind stress (positive values of τ^x) which is down-front to the mean flow in direction. Similarly, easterly winds are considered up-front (negative values of τ^x) as these winds oppose the direction of the mean geostrophic flow. We acknowledge this is only a representation of the mean sense of the flow where there may be misalignment with our estimates of down-front winds and the true direction of the local front. The glider sampling strategy was to direct the glider toward 0°E and as such the true strength of the front, when occupying a meridional orientation, is likely underestimated.

Importantly, the competition between the restratification processes of MLEs, which are inherently positive, and EBF (equation (2)), which can be positive or negative, sets the equivalent heat fluxes, which compete with solar heating to define the stratification of the ML.

3. Results and Discussion

3.1. In Situ Observations: Characterizing the Seasonal Variations of the SAZ Mixed Layer

The 5 month glider experiment encompasses two seasonal regimes where, the upper ocean temperature environments show distinct differences (Figure 2). This is illustrated in Figure 2a, where a southward migration of surface warming across the location of the glider occurs as the time series progresses, thus separating the spring and summer periods. Although this is a gradual process, the location of the glider relative to this warming allows a defined date of spring/summer separation, on 28 November [*Swart et al*., 2015]. This date corresponds to where surface warming (indicated by the 11°C isotherm in Figure 2b) drives the development of a thermocline originating from the surface, which merges with the deeper "seasonal"

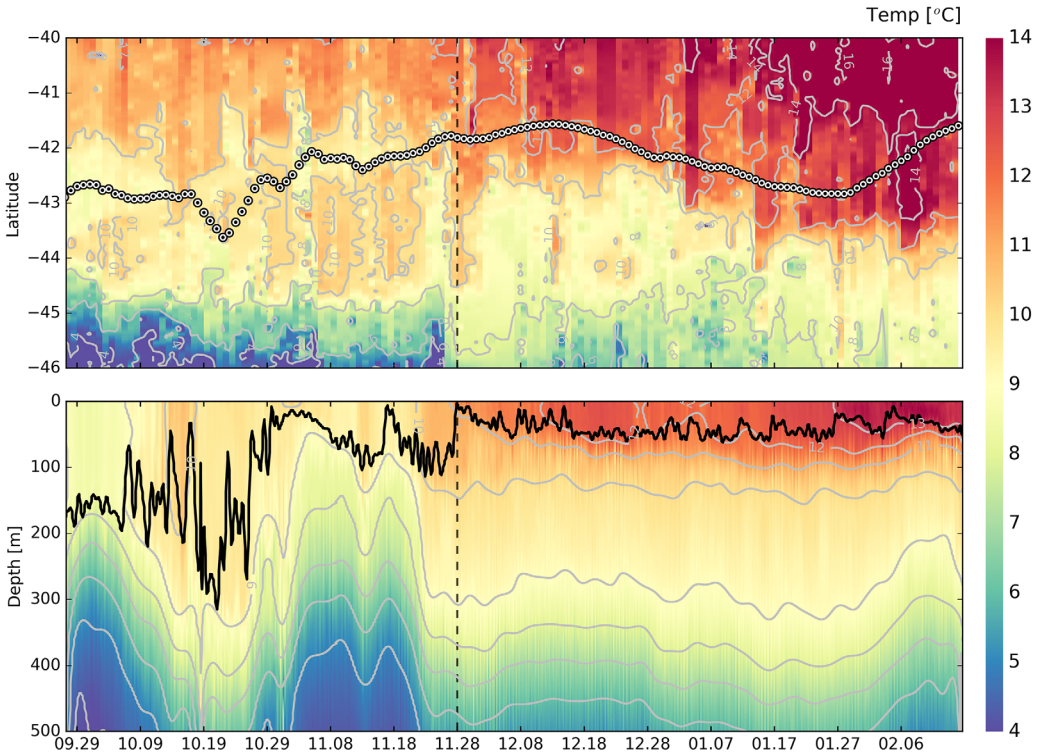

Figure 2. (top) Hovmöller representation of the seasonal progression of SST (°C). Black dots indicate the daily mean SG573 location. The first period of sampling (deployment to 28 November, which is indicated by the vertical dashed line) can be characterized by mesoscale, synoptic warming events extending up to 2° latitude southwards, while the second period (latter half of the time series) is dominated by the seasonal southward progression of warming SST. (bottom) Depth-time temperature section from SG573 where the feature driven environment during the first half of sampling dominates the MLD (black line) variability. Gray lines indicate isotherms for top and bottom plot.

thermocline (Figures 3 and 4 in *Swart et al*. [2015]) to form the base of the ML for the remainder of the time series. Figure 3 displays the ML temperature and salinity variations scaled to show equal contributions to changes in density. Here, the separation between the spring and summer ML regimes is clear. ML temperature and salinity variations on density were compensated for extended periods during spring, while surface warming during summer continually increased the buoyancy of the ML more so than ML freshening. The authors propose that the date of the seasonal transition from deep MLDs during spring to shallow MLDs during summer is not consistent throughout the SAZ. It is likely that zonal asymmetry in surface heat fluxes and MLDs provide different seasonal restratification dates [*Sallée et al*., 2010].

During spring, varying phases lasting less than a week, and approximately 3 weeks show that variations of ML temperature and salinity compensate to have no, or little effects on density (see gray shading in Figure 3). Meanwhile, interspersing periods have temperature and salinity variations which do not compensate each other (see green shading in Figure 3). In such cases, increasing temperature and/or freshening of the ML enhance the buoyancy, changing density of the ML. Meanwhile during summer, the near-persistent increase in temperature and gradual decline in salinity indicate a completely contrasting environment where the ML becomes increasingly buoyant with time. In the following two subsections, we separate and examine the spring and summer periods individually to provide intraseasonal evaluations of upper ocean physical variability in the SAZ.

3.1.1. Spring: October–December

Figure 2a indicates that the glider was deployed within the zone of 9°C SST water. As time progressed, episodic events whereby surface waters warmed up to 2°C were observed. These signatures represent synoptic scale warming extending up to 2° of latitude in the SST. The glider temperature depth section indicated that these warming events extend vertically throughout the ML (Figure 2b, e.g., mid-October and mid-November), driving temperature and salinity ranges of 8.5–11°C and 34.3–34.8 during spring (Figure 3). ML temperature and salinity varied as rapidly as 0.8°C d^{-1} and 0.2 d^{-1}, respectively. Longer scale changes of the upper ocean temperature structure spanning numerous weeks were reflected in the vertical

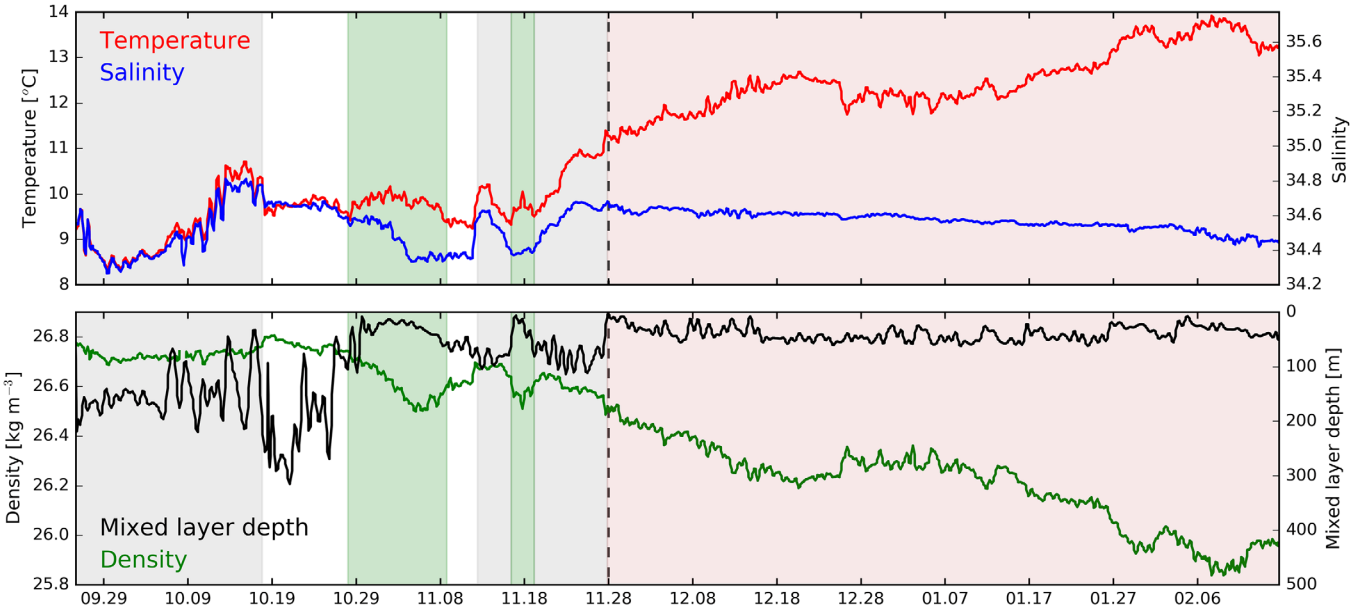

Figure 3. (top) Mixed layer temperature (red line) and salinity (blue line) variations throughout the glider time series. The vertical axes are scaled by α (temperature) and β (salinity) so that variations in T and S have equal effects on density. Spring and summertime periods are separated on 28 November by the dashed vertical line; hereafter temperature dominates the variations to density. Gray-shaded areas indicate where density-compensated changes in T and S occur while green shading depicts where variations in either T or S alter mixed layer density. White areas represent insignificant variations in T and S. (bottom) Mixed layer density (green line) and depth (black line). Shading as is in the top plot, where variations in ML density during the green-shaded periods are synonymous with MLDs below 100 m.

displacement of isotherm depths by approximately 200 m. This was noticeable in November by a distinct doming of the 5–9°C isotherms (Figure 2b). It is likely this type of variability was imparted by a combination of time-varying forcing mechanisms altering the physical properties of the ML and variations of the glider location as a result of the sampling strategy. Therefore, this data set demonstrates multiscale upper ocean variability, ranging from the rapid daily variations to the longer weekly synoptic scales.

Owing to its highly energetic nature, mesoscale eddies in the Southern Ocean are prevalent. The glider was deployed directly west of a cold-core cyclone of diameter ~200 km, which may have broken off from a meander of the Subantarctic Front. The glider performed a direct crossing of the cyclone during the first 2 weeks of the deployment (Figures 4a–4c). A vertical section of upper ocean temperature as the glider crossed the eddy is shown in longitudinal space (Figure 4d). Classical doming of the isotherms toward the warmer edges of the cyclone were seen, with characteristic upwelling through the eddy core, as seen by a temperature and salinity reduction in the center to the coldest (8–9°C) and most fresh (34.3–34.4) for the entire experiment. The ML density (26.6–26.7 kg m^{-3}) was characteristic of Subantarctic Mode Water [*McCartney*, 1982]. Despite the temperature and salinity gradients across the eddy, their relative effects on density were mostly compensated and thus horizontal density gradients were weak.

Contrasting dynamic exists where variations of ML temperature and salinity were not compensated and thus changes in temperature and/or salinity alter the density of the ML (Figure 3). This occurred from 29 October for 2 weeks (green-shaded areas of Figure 3), where warming and freshening resulted in less dense MLs and shallowing of the MLD from >200 m to below 100 m. The interest of this study is to investigate these processes and identify their role in setting the stratification of the upper ocean, especially during these noncompensated regimes, where horizontal density gradients may play an important role in ML physical dynamics.

3.1.2. Summer: December–February

Regional surface warming and shallow (<100 m) MLDs are typical for this region and season [*Sallée et al.*, 2010]. *Swart et al.* [2015] found a strong connection between ML deepening and enhanced wind stress events related to midlatitude storms varying at the synoptic scale (4–9 days). Further attention is needed to assess the influence of horizontal submesoscale processes on the MLD variability during this time. Our observations indicate the regional context of glider sampling trajectory moving southward for the majority of the summer (December–February) at around the same rate as the southward propagation of surface

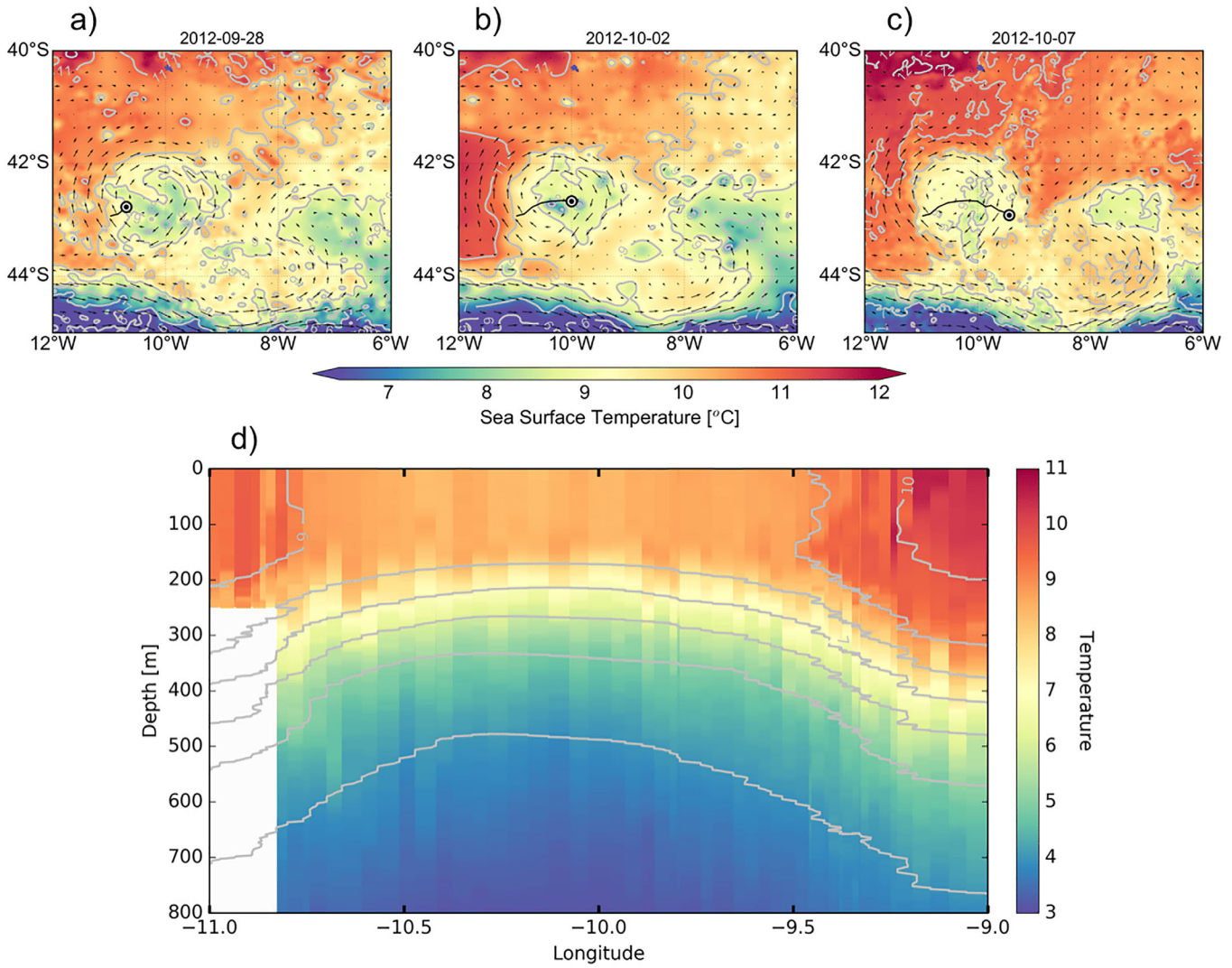

Figure 4. (a) Series of three daily SST maps indicating the cyclone (~43°S, 10°W) crossed by the glider track (white-black dots). Arrow indicate AVISO surface velocities. (b) Vertical temperature section of the black glider line shown in the third SST plot (7 October).

warming, i.e., southward migration of outcropping isotherms (Figure 2a). This results in an underestimation of the seasonal warming which would likely occur at a single location over the season. Nevertheless, a comparison of the seasonally averaged temperature profiles in Figure 5 indicates the upper 50 m warmed by approximately 2.5°C from spring to summer. Additionally, vertical variations of the MLD are indicated in Figure 5 by measure of the standard deviation for each season, where a reduction from 79 to 16 m occurred from spring to summer. These correspond well to the estimates made for the entire Southern Ocean, which represent the large-scale seasonal variations in heating and its effects on upper ocean variability [*Sallée et al.*, 2010]. Interestingly, despite the reduction of the MLD and its variability during summer, standard deviations of the ML temperature were comparable between spring (0.63°C) and summer (0.64°C) (Figure 5). This indicates that the processes impacting the subdaily upper ocean temperature variations were present during spring and summer.

Sharp variations of ML density occurred during periods where temperature and salinity variations were large (Figure 6). These rapid changes in density were aligned with temporal variations associated with submesoscale variability, i.e., within a few days. These can be identified as "sharp" periods of lighter and denser surface waters which occurred frequently throughout the time series, often resulting in ML density changes up to 0.1 kg m^{-3} d^{-1} (Figure 6). At these locations, upper ocean stratification, taken as the average N^2 over the top 100 m, show weakening during phases of denser MLs and strengthening during periods of lighter

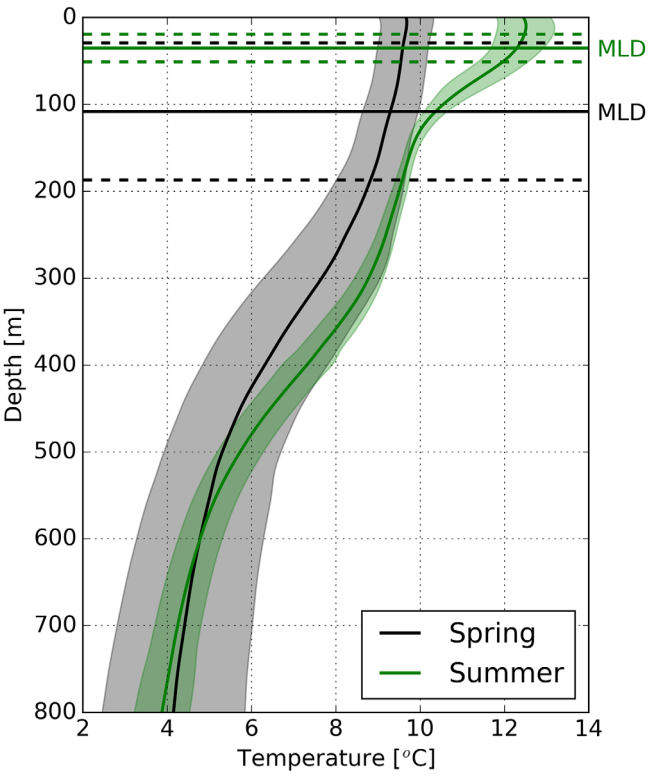

Figure 5. Mean temperature profiles for spring (25 September to 28 November) and summer (29 November to 15 February) shown as thick black and green lines, respectively. Standard deviations of the temperature at each depth are represented as the shaded areas. The mean MLD for each season is shown by the horizontally orientated solid lines, with one standard deviation shown above and below the MLD as the dashed lines.

MLs. Notably, during green shades areas of Figure 6, MLs rapidly became less dense while the ML began to restratify. Similarly, the increase of ML density resulted in the destruction of stratification, e.g., during mid-November. As MLEs actively slump vertical isopycnals in the presence of large horizontal density gradients to restratify the water column and EBF advects heavier water over lighter water to mix the upper ocean, it is postulated that submesoscale processes are likely important in altering the upper ocean stratification. However, it needs to be considered that these changes in density and stratification may be the result of air-sea heat and momentum exchange imparting intraseasonal variability on ML temperature through warming (less dense) and mixing (more dense), such as would be modulated by synoptic scale winds. Therefore, to investigate the role of 1-D air-sea exchange processes on the observed stratification, such as wind and surface heat flux, we employ the 1-D PWP model with the observed 1-D forcing parameters. We compare the stratification derived by the 1-D processes to the observed ocean stratification to separate the 3-D processes from the 1-D domain.

3.2. 1-D model Comparison: Atmospheric Parameters

The model is forced with meteorological data acquired at the time and location of the nearest glider profile. Winds varied at the synoptic scale (Figure 7a), indicative of the storm-like activity in the Southern Ocean [*Trenberth*, 1991]. This indicates that the glider moves slowly in comparison to the regional trajectory of the Southern Ocean storms and can therefore sample the effects of the storms on the water column. A mean

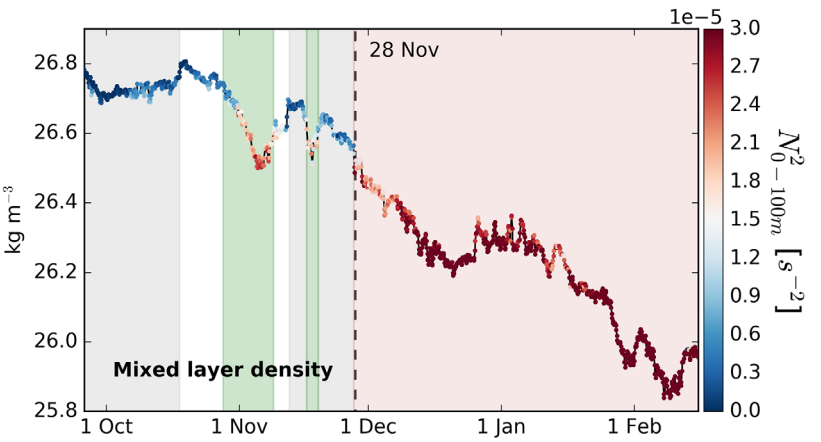

Figure 6. Density averaged over the ML for the entire glider data set. Gradual decline in ML density represents the impact of seasonal warming of the upper ocean. Colors are a representation of the stratification (N^2) averaged for the upper 100 m of the ocean. Green-shaded areas show where enhanced upper ocean stratification agrees with ML density becoming less dense. Shading as in Figure 3.

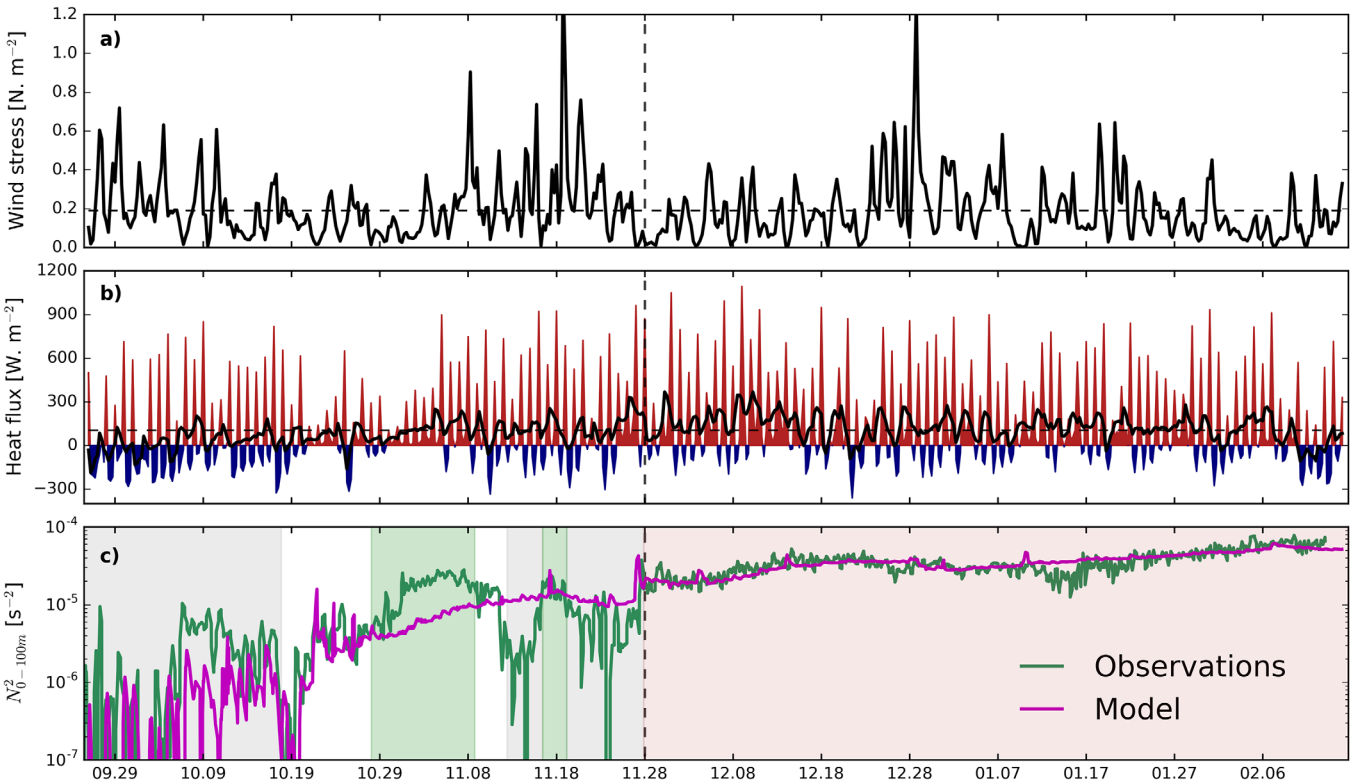

Figure 7. (a) NCEP wind stress (N m^{-2}) colocated to the time and position of glider profiles and used for the PWP model run. (b) MERRA 6 hourly net heat flux (Q_{NET}) at the ocean surface (red (blue) indicates ocean heating (cooling)) indicates a strong diurnal structure with a net positive heat flux into the ML. (c) Time series of stratification (N^2) averaged for the upper 100 m for SG573 (green line) and the PWP model (magenta line). Shaded areas are as in Figure 3.

wind stress of 0.19 N m^{-2} was recorded, while two extreme storms intercepted the glider during mid-November and late-December, where wind stress values exceeded 1 N m^{-2}.

Surface heat flux variations (Figure 7b) were characterized by a strong diurnal signal. Strong cooling periods (−300 W m^{-2}) were dominated by intense heating regularly exceeding 800 W m^{-2}. A mean positive Q_{NET} (104 ± 281 W m^{-2}) indicated a net input of buoyancy to the surface of the ML throughout the model simulation. These heat, momentum (Figures 7a and 7b), and freshwater (not shown) fluxes were used to force the PWP model for 143 model days.

3.2.1. Seasonal Mixed Layer Restratification by Model and Glider Observations

In our observations, springtime restratification developed as a stratification emerging from the surface of the ocean. This is distinct from a shoaling of the seasonal pycnocline. The transition into summer was signified by a merging of the seasonal pycnocline with the springtime restratification at approximately 50 m, forming the MLD for the remainder of summer shallower than 100 m (Figure 3 in *Swart et al.* [2015]). Therefore, we use the stratification index N^2, where $N^2 = \frac{-g}{\rho_0}\frac{\partial \rho}{\partial z}$, averaged over the top 100 m of the water column ($N^2_{0-100\mathrm{m}}$) to provide an understanding of the development in seasonal restratification. Figure 7c shows the direct comparison of the $N^2_{0-100\mathrm{m}}$ between the PWP model and the glider observations. The majority of October exhibited weak stratification. However, small, significant increases of glider-observed stratification ($N^2_{0-100\mathrm{m}}$ 0.5–1 × 10^{-5} s^{-2}) were found around 9 October, which remained absent in the model. Weak heating and intermittent wind stress bursts of over 0.6 N m^{-2} likely provided sufficient near-inertial shear to prevent the upper ocean from stratifying. Additionally, this period coincides with the glider exiting the mesoscale cyclone. Interleaving water masses of the cyclone and ambient water could potentially provide stratification by small density changes between water masses undergoing a release of available potential energy (Figure 3).

From 28 October to 9 November, low winds often below 0.2 N m^{-2} positive surface heat fluxes enhanced the model and observed ocean stratification. However, the ocean restratification increased at a rate much

larger than the simulated stratification, whereby within 1 week (4 November), the strength of the observed stratification more than doubled the model estimate, with in situ N^2_{0-100m} reaching $\sim 3 \times 10^{-5}$ s^{-2} (Figure 7c).

From 8 November, the observed stratification was readily reduced from $\sim 3 \times 10^{-5}$ s^{-2} to almost zero in about 1 week. The model stratification, albeit much weaker, continued to steadily increase despite wind stress increasing to above 0.8 N m^{-2} (Figure 7c). The overlaid shaded areas in Figure 7c represent the various regimes of ML temperature and salinity variations found in Figure 3. Interestingly, noncompensated temperature and salinity variations resulted in a rapid increase of the observed stratification, greatly exceeding the model estimates, while compensated variations indicated a well-mixed upper ocean with weak observed stratification (gray shading in Figure 7c). At the onset of summer (28 November), the modeled and observed stratification were comparable ($N^2_{0-100m} \sim 2 \times 10^{-5}$ s^{-2}). Strong heating during summer (>400 W m^{-2}) far exceeded cooling of the ML surface, which only fell below −200 W m^{-2} once in 3 weeks. This resulted in a simultaneous increases of stratification in the model and observations. From 23 December, a series of storms with elevated wind stress above 0.4 N m^{-2}, reaching up to 1.2 N m^{-2} provided sufficient vertical shear-mixing in both the model simulation and the ocean leading to decreased N^2_{0-100m} by 1×10^{-5} s^{-2} in the model and 2×10^{-5} s^{-2} in ocean observations.

The freshwater fluxes incorporated in the PWP model influence primarily the summertime stratification. Rainfall in the SAZ occurs periodically with peaks over 6 mm d^{-1}, reaching up to 12 mm d^{-1} during the maximum rainfall event. These instantaneous events do not significantly impact the modeled stratification. However, a model simulation with rainfall turned off (not shown) suggests that without rainfall, the summer stratification would be weaker than what the model and glider observations suggest. This could have notable implications for upper ocean stratification should climate variability in rainfall patterns impact precipitation in the SAZ, or if precipitation belts shift meridionally in relation to the Southern Annular Mode [e.g., *Gillett et al*., 2006; *Hendon et al*., 2014] or other climate modes of variability.

To test whether the variability of the observed stratification was a result of the glider moving across gradients of physical properties which exhibit contrasting upper ocean stratification, the model was initiated at three-independent periods throughout the time series. These include prior to the onset of spring restratification, during the period where spring restratification was strongest, and the beginning of summer (not shown). These time were chosen selectively as each one represents contrasting stratification. The stratification for each simulation showed minor differences in magnitude, depending on the strength of the stratification during the model initiation. However, the variability of stratification remained comparable to the model run shown in this work, suggesting that the glider does not sample across horizontal gradients of vertical stratification, and moves at a rate slow enough to capture the evolution of the observed stratification.

Previous work to understand seasonal restratification of the ML has shown that 1-D processes may explain springtime increases in stratification such that that the onset of seasonal heat gain imparts an immediate shallowing of the MLD, which can be subsequently mixed by a passage of storms acting to vertically homogenize the water column [*Waniek*, 2002]. The results shown by the 1-D model propose the timing of seasonal restratification in the SAZ can be linked to surface heat, freshwater, and momentum fluxes as stratification goes hand in hand with heating in the late spring. This may have important implications for regions of weak ocean energetics, as is seen in *Babu et al*. [2004]. However, the Southern Ocean is a turbulent environment [*Naveira Garabato et al*., 2004] fostering well-known frontal regions separating water masses of varying buoyancy characteristics [*Orsi et al*., 1995] and here we show that shear-driven mixing and entrainment are not solely responsible for the variability of the springtime upper ocean restratification SAZ as the susceptibility of upper ocean stratification to undergo rapid and large variations is under-represented by the model. Therefore, this model experiment provides evidence that our understanding of upper ocean variability in the Southern Ocean requires the implementation of processes not represented in a 1-D framework.

Our observations were taken in the SAZ south of Africa, where lighter water from the subtropics meets colder, denser water from the Subantarctic-Antarctic. We show this region exhibits various regimes in ML variability. During periods where temperature and salinity do not compensate in their contribution to density, deviations of stratification between the model and observations were greatest. These periods were synonymous with less dense MLs and enhanced stratification in the observations (Figure 6), whereas the

simulated stratification showed a much weaker but more gradual increase with time. Therefore, the results from the PWP model suggest these less dense MLs were not solely driven by surface heat fluxes.

1-D models cannot be expected to provide complete simulations of Southern Ocean dynamics, as advective fluxes and other 3-D processes are important to its upper ocean variability. For example, the PWP model lacks the provision for the vertical displacement of the thermocline due to internal gravity waves, and is mainly influenced by bulk and gradient Richardson mixing and not accounting for diffusion occurring between the ML and below (that could still be significant, *Nicholson et al.* [2016]). It is important to understand the processes which drive these ML changes as they have implicit implications on ML stratification and further biogeochemical responses [*Swart et al.*, 2015]. Thus, we propose that the 3-D processes not resolved in the model may have large-scale implications across the Southern Ocean where horizontal gradients exist, and thus have an key role in explaining the enhanced springtime stratification variability in the Subantarctic Ocean. To investigate the role of submesoscale processes during the seasonal onset of ML restratification, we apply parameterizations developed in numerical studies to estimate the equivalent heat fluxes applied to the ML by submesoscale processes [*Fox-Kemper et al.*, 2008; *Mahadevan et al.*, 2010]. We look to scale the potential fluxes imparted by upper ocean instabilities derived by enhanced horizontal buoyancy gradients to explain the departure between our observations and the model.

3.3. The Impact of Submesoscale Processes in Defining the Mixed Layer Stratification

To better understand the role of submesoscale processes in the seasonal restratification of SAZ ML, we require observations of the horizontal buoyancy gradients (b_y) sampled between glider dives. It is reasonable to assume the glider sampled the submesoscale as the mean distance between profiles was 1.4 km $\pm$ 0.9 km, well within the typical range of the Rossby radius of deformation ($\sim$10 km). However, submesoscale processes develop rapidly (within days) and thus we may only observe the end result of a process which has already occurred.

As the sampling strategy for this experiment was to direct the glider trajectory predominantly eastward to remain in the SAZ, the glider-derived b_y is a better representation of the meridional-orientated fronts rather than the large zonal fronts of the ACC. Therefore, estimating the equivalent heat fluxes of MLEs and wind-driven surface forcing using a glider may result in over and under-estimations due to variations in the alignment of the glider path, the front and the wind direction. Figure 15 of *Thompson et al.* [2016] estimates the EBF using all possible angles of the glider dive, wind orientation, and horizontal buoyancy gradient. They show that Q_{Ekman} will represent almost all, or very little of the actual equivalent heat fluxes depending on the orientation of the wind, glider path and front. However, the root-mean-square of observed EBF to the actual EBF is 0.71, indicating that over the duration of a season, our estimation of submesoscale fluxes is likely to result in an underestimation of the effects of Q_{MLE} and Q_{Ekman} on the ML stratification.

The meridional direction of each glider dive continually varied during this experiment. Thus, the sign of the horizontal buoyancy gradients sampled is likely to have arbitrary orientation depending on the direction of the dive. This complication is important when considering front-wind orientation. Therefore, the sign of b_y was modified to represent the meridional orientation of the front. Fronts with lighter water to the north were made positive. Albeit the dominant sampling direction was eastward, the sign of the zonal component of the fronts was chosen to be modified as opposed to the meridional component owing to the wind direction being dominated by the westerlies. This makes it possible to elucidate whether the wind direction was orientated up or down the submesoscale front. For example, a westerly wind with a positive b_y indicates a down-front wind. We acknowledge this may not provide exact down or up-front wind orientation as meridional-orientated fronts will be underestimated and EBF overestimated, however it provides some clarity of the direction of the front in relation to the dominant zonal wind orientation. Finally, the impacts of changes in wind stress and wind direction on upper ocean stratification are provided.

The time series of glider estimated b_y along its path is shown in Figure 8a. Weaker ML horizontal buoyancy gradients ($b_y < 0.5 \times 10^{-7}$ s^{-2}) were observed during the first month of the time series, particularly when the MLD was deep (>200 m). Meanwhile, within shallow MLDs (<100 m) during spring, periodic fluctuations of enhanced horizontal buoyancy gradients were observed ($b_y > 0.5 \times 10^{-7}$ s^{-2}). During spring, these were often far reaching, extending down to 400 m. However, during summer, elevated b_y at the base of the MLD was limited to the depth of the pycnocline. This is likely an artifact of an internal wave process

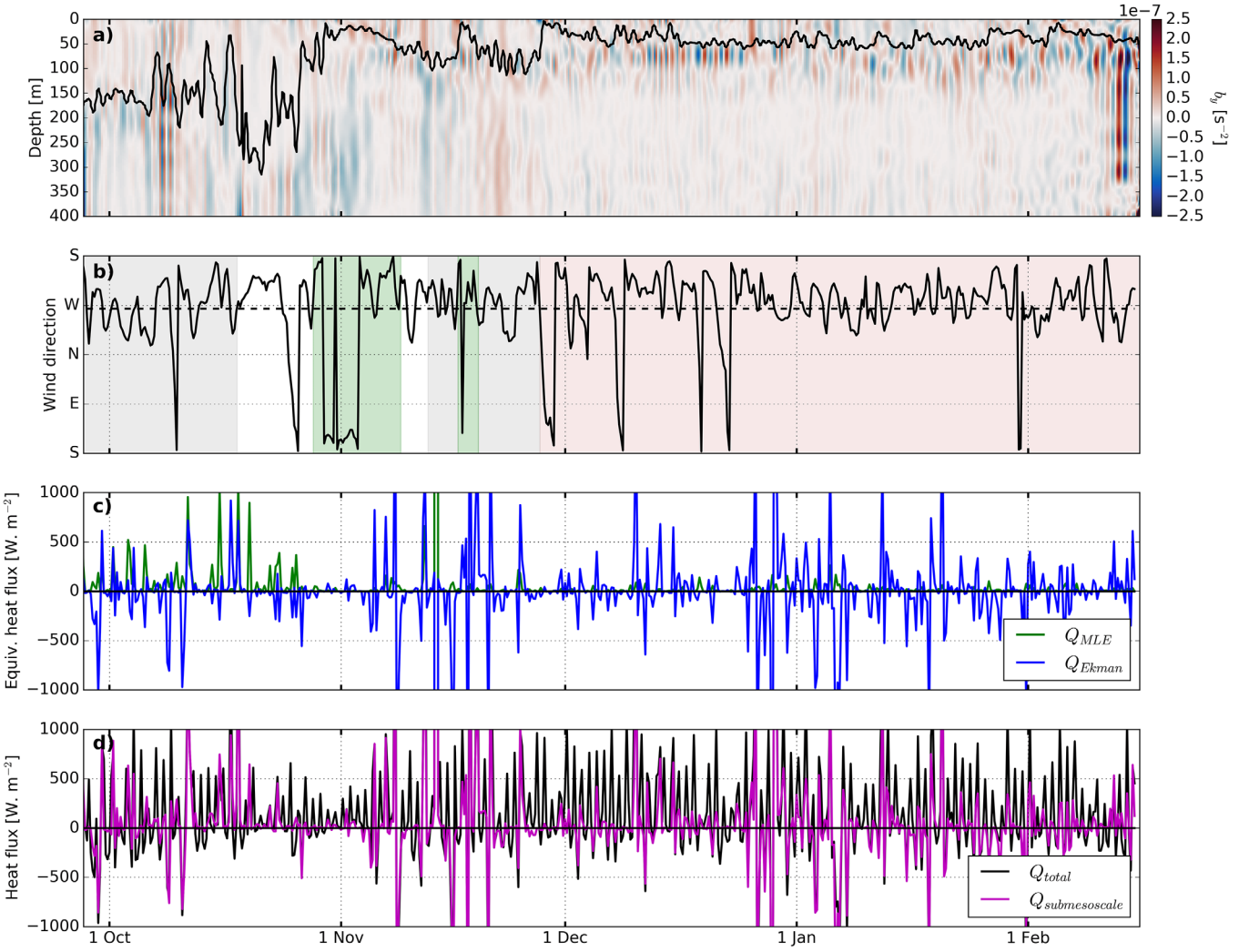

Figure 8. (a) Glider observed horizontal buoyancy gradients b_y (s^{-2}; color) with MLD (m) overlaid with a black line. (b) Wind direction obtained at each wind measurement. Shaded areas are as in Figure 3. (c) Equivalent heat flux values of Q_{Ekman} (blue line) and Q_{MLE} (green line) indicate the competition between wind-driven EBF and ML eddies. (c) Equivalent heat flux values of $Q_{submesoscale}$ (the sum of Q_{Ekman} and Q_{MLE}), and the combined total of all three fluxes (black line).

vertically displacing the pycnocline and the glider sampling as a function of space and time [*Thompson et al.*, 2016].

Equivalent heat flux estimates of Q_{MLE} and Q_{Ekman} are calculated by equations (1) and (2), respectively, and are depicted in Figure 8c. Q_{MLE} is observed to be largest during the spring when the MLD is deeper than 100 m, with periodic spikes up to 1000 W m^{-2}. These MLE fluxes are representative of the horizontal buoyancy gradient sampled by the gliders path, therefore, it is likely that these b_y values are underestimated and that Q_{MLE} is higher in reality. As the periods of restratification exhibited shallow MLDs ($<$100 m), estimates of Q_{MLE} were weak ($<$200 W m^{-2}). As such, values of Q_{MLE} after the springtime restratification were weak and the effects of MLE negligible. Although large periodic fluxes of Q_{MLE} occurring during deep MLDs suggest they may be important in enhancing the stratification, the onset of restratification occurred as the wind direction changed from a predominantly westerly wind during the initial month of the time series, to southerly wind persisting for a number of days (Figure 8b). Synonymously, the wind stress weakened to below 0.2 N m^{-2} while Q_{Ekman} reduced to $<$100 W m^{-2}.

Mahadevan et al. [2012] provide a ratio of buoyancy fluxes due to down-front winds and MLEs by $R = \frac{\tau^x}{C_e \rho_0 b_y H^2}$, where τ^x is the down-front wind stress, H is the MLD and $C_e = 0.06$. Where $R = 1$, the effects of restratification by MLEs and destratification by EBF equally oppose each other. For typical spring value of

$b_y = 1 \times 10^{-7}$ s^{-2} with a MLD of 150 m, τ corresponds to 0.14 N m^{-2}. The wind reversal and subsequent weakening of the wind stress toward the end of October satisfy these conditions which allow restratification of the MLD by MLEs. A successive passage of storms from early November (Figure 7b) enhanced the down-front winds (>0.4 N m^{-2}) to generate intense negative Q_{Ekman} larger than −1000 W m^{-2}, providing conditions whereby EBF dominated the restratification by MLEs and surface heat fluxes (Figure 8d). The MLD subsequently deepened from 20 to 150 m over 6 days of down-front persistent winds (Figure 8a). This resulted in the eradication of N^2_{0-100m} in the observations which were not explained by shear-driven mixing alone (Figure 7c).

In our observations, the springtime restratification rapidly shoals the MLD from >200 m to <100 m within a few days. Prior to this restratification, the equivalent heat flux by submesoscale processes (combination of Q_{MLE} and Q_{Ekman}) approached 1000 W m^{-2} at times (Figure 8d), dominating the contribution to the combination of surface heat fluxes and equivalent submesoscale fluxes (Figure 8c). During down-front winds, EBF dominates the restratifying flux by MLEs. However, weakening winds during wind reversals away from the nominally down-front wind conditions allow MLEs to dominate. The high values of horizontal buoyancy gradients and deep MLDs prior to the spring restratification of the ML implicate that MLEs may provide an important mechanism to support the seasonal restratification of the ML. We expect values of Q_{MLE} to be greater during winter, due to deeper MLDs enhancing the available potential energy in the ML [*Callies et al*., 2015; *Thompson et al*., 2016]. A full seasonal cycle (winter-summer) would present more information to understand the presence of submesoscale flows in the Southern Ocean.

Our observations agree with those of *Mahadevan et al*. [2012], where MLEs are potentially important during springtime restratification. However, our results indicate that MLEs act in combination with a positive surface heat flux and a weakening of the local wind stress to restratify the upper ocean, while the North Atlantic study focuses primarily on the value of Q_{NET} as the mediator of MLE restratification. *Thompson et al*. [2016] perform a full seasonal cycle of glider measurements in the North Atlantic, and show that the same submesoscale processes shown here can reverse the sign of heat fluxes up to 25% of the time during winter, providing a restratification flux which can oppose winter cooling. Although ever present horizontal buoyancy gradients in the Southern Ocean suggest that submesoscale flows may be prevalent in winter, intense cooling and strong down-front winds shown in this work may inhibit such flows to undergo ML restratification.

The potentially important role of submesoscale flows in periodically increasing, or decreasing the total net heat flux applied to the Subantarctic ML during the springtime restratification may have far reaching implications in our understanding of how the open ocean Southern Ocean responds to increased heating and winds. Understanding these processes is fundamental as *Swart et al*. [2015] indicate that the observed spring restratification is consistent with an increase in primary production. Additionally, strong intraseasonal variability in primary productivity and carbon fluxes has been discussed in a number of recent studies for this region [*Thomalla et al*., 2011, 2015; *Swart et al*., 2015; *Carranza and Gille*, 2015; *Monteiro et al*., 2015; *Nicholson et al*., 2016]. *Thomalla et al*. [2011] first showed that large regions of the Southern Ocean experience regional heterogeneity in the seasonal onset of phytoplankton blooms. The sensitivity of submesoscale processes to heating, wind stress, and direction shown here suggest that they may be important in determining the timing of these blooms and associated CO_2 flux. Although submesoscale processes may only be dominant for only a few weeks during the end of spring, their impacts on upper ocean stratification may have critical implications given the large extent of the Southern Ocean. In addition, the frontal regions of the Southern Ocean are prone to stronger horizontal buoyancy gradients, and thus submesoscale flows may be augmented throughout other periods of the seasonal cycle for these areas.

Additionally, Q_{Ekman} can reverse the sign of the net surface heat flux into the ML from a positive to a negative during strong down-front winds (Figure 8d), which may provide an additional mixing dynamic to 1-D shear-driven mixing. Considering the vast uptake of CO_2 by the Southern Ocean as a result of primary production, it is important that we fully understand these processes over a full seasonal cycle, especially in the interest of parameterizations in climate models.

Future development of this work will look to implement 3-D modeling suitable for the SAZ to enhance our understanding of the evolutionary processes that develop between MLE, along-front winds and heating/cooling where the influence of these processes on net seasonal primary productivity and associated carbon

cycling are likely to be important. Furthermore, full seasonal observations (winter to summer; currently underway through the SOSCEx III glider deployments) will help to explain the seasonality of submesoscale processes in the Southern Ocean and their associated impacts on the ML variability.

4. Conclusions

In this study, we applied 5 months of high-resolution ocean glider data from the SAZ to investigate the processes that determine the transition from a weakly stratified upper ocean during the springtime to a strongly stratified shallow ML environment in summer. Simulations from a 1-D mixing model indicate that 1-D fluxes of heat, freshwater, and momentum can explain the timing of seasonal restratification. However, 1-D fluxes alone cannot explain the observed magnitude and variability of the springtime restratification. The glider data show the presence of strong submesoscale buoyancy fronts within the ML during spring. Under weak down-front winds or up-front wind reversals, in the presence of submesoscale buoyancy fronts and deep MLDs, the ML is conducive to restratification by MLEs. This timing of enhanced MLE fluxes is able to explain the observed variations of stratification that 1-D processes cannot. These observations suggest that submesoscale processes play an important role in enhancing the seasonal restratification of the ML where a separate study using the biogeochemical properties from this data set show this period to be key in the seasonal increase of primary production [*Swart et al*., 2015]. Future work will focus on understanding the vertical motions between the ML and the ocean interior as this provides crucial information about nutrient transport supporting summer phytoplankton blooms. Additionally, the implementation of 3-D numerical simulations applying characteristics of the SAZ will assist to quantify the evolutionary process of submesoscale dynamics and MLEs and their associated impact on biogeochemical cycles in this globally important region.

Acknowledgments

The authors would like to thank an anonymous reviewer for the helpful comments and for the time taken to help us improve this manuscript. The authors of this work would like to thank SANAP and the captain and crew of the *S.A. Agulhas I* and *S.A. Agulhas II* for their contribution in the deployment and retrieval of the Seagliders during SOSCEx. We acknowledge the work of SAMERC-STS for housing, managing, and piloting the gliders. M. du Plessis would like to thank those at WHOI who facilitated two Guest Studentships, which enhanced this work and also to Jennifer Jackson-Veitch for her support during this study. The South African ocean glider program is supported by the Department of Science & Technology (DST) through the Sustainability & Innovation in Southern Ocean Observational Infrastructure grant. S. Swart was supported by the South African NRF-SANAP, grant SNA14071475720 and a Wallenberg Academy Fellowship. Lastly, S. Swart thanks the numerous technical assistance, advice and IOP hosting provided by Geoff Shilling and Craig Lee of the Applied Physics Laboratory, University of Washington. AM thanks NSF for support under grant OCE-I434788. The glider data used in this work are available at the National Centers for Environmental Information (https://www.ncei.noaa.gov/)

References

Babu, K. N., R. Sharma, N. Agarwal., V. K. Ajarwal, and R. A. Weller (2004), Study of the mixed layer depth variations within the north Indian Ocean using a 1-D model, *J. Geophys. Res.*, *109*, C08016, doi:10.1029/2003JC002024.

Boccaletti, G., R. Ferrari, and B. Fox-Kemper (2007), ML instabilities and restratification, *J. Phys. Oceanogr.*, *37*(9), 2228–2250, doi:10.1175/JPO3101.1.

Callies, J., R. Ferrari, J. M. Klymak, and J. Gula (2015), Seasonality in submesoscale turbulence, *Nat. Commun.*, *6*, 6862, doi:10.1038/ncomms7862.

Carranza, M. M., and S.T. Gille (2015), Southern Ocean wind-driven entrainment enhances satellite chlorophyll-a through the summer, *J. Geophys. Res. Oceans*, *120*, 304–323, doi:10.1002/2014JC010203.

Caulet, C., S. Swart, and M. Rouault (2015), Comparison of in-situ heat flux measurements with satellite re-analysis products of the Southern Ocean, Master's thesis, Univ. of Cape Town, Cape Town.

D'Asaro, E., C. Lee, L. Rainville, R. Harcourt, and L. Thomas (2011), Enhanced turbulence and energy dissipation at ocean fronts, *Science*, *332*(6027), 318–322, doi:10.1126/science.1201515.

de Boyer Montégut, C., G. Madec, A. S. Fischer, A. Lazar, and D. Iudicone (2004), Mixed layer depth over the global ocean: An examination of profile data and a profile-based climatology, *J. Geophys. Res.*, *109*, C12003, doi:10.1029/2004JC002378.

Forryan, A., A. C. Naveira Garabato, K. L. Polzin, and S. Waterman (2015), Rapid injection of near-inertial shear into the stratified upper ocean at an Antarctic Circumpolar Current front, *Geophys. Res. Lett.*, *42*, 3431–3441, doi:10.1002/2015GL063494.

Fox-Kemper, B., R. Ferrari, and R. Hallberg (2008), Parameterization of ML eddies: Part I: Theory and diagnosis, *J. Phys. Oceanogr.*, *38*(6), 1145–1165, doi:10.1175/2007JPO3792.1.

Gillett, N. P., T. D. Kell, and P. D. Jones (2006), Regional climate impacts of the Southern Annular Mode, *Geophys. Res. Lett.*, *33*, L23704, doi:10.1029/2006GL027721.

Haine, T. W. N., and J. Marshall (1998), Gravitational, symmetric, and baroclinic instability of the ocean mixed layer, *J. Phys. Oceanogr.*, *28*, 634–658, doi:10.1175/1520-0485(1998)028 < 0634:GSABIO > 2.0.CO;2.

Hendon, H., E. Lim, and H. Nguyen (2014), Seasonal variations of subtropical precipitation associated with the southern annular mode, *J. Clim.*, *27*, 3446–3460, doi:10.1175/JCLI-D-13-00550.1.

Hosegood, P., M. C. Gregg, and M. H. Alford (2006), Sub-mesoscale lateral density structure in the oceanic surface mixed layer, *Geophys. Res. Lett.*, *33*, L22604, doi:10.1029/2006GL026797.

Large, W. G., and S. Pond (1981), Open ocean momentum flux measurements in moderate to strong winds, *J. Phys. Oceanogr.*, *11*(3), 324–336, doi:10.1175/1520-0485(1981)011 < 0324:OOMFMI > 2.0.CO;2.

Mahadevan, A., A. Tandon, and R. Ferrari (2010), Rapid changes in ML stratification driven by submesoscale instabilities and winds, *J. Geophys. Res.*, *115*, C03017, doi:10.1029/2008JC005203.

Mahadevan, A., E. D'Asaro, C. Lee, and M. J. Perry (2012), Eddy-driven stratification initiates North Atlantic spring phytoplankton blooms, *Science*, *337*(6090), 54–58, doi:10.1126/science.1218740.

McCartney, M. S. (1982), The subtropical recirculation of mode waters, *J. Mar. Res.*, *40*, supplement, 427–464.

Monteiro, P., L. Gregor, M. Lévy, S. Maenner, C. L. Sabine, and S. Swart (2015), Intraseasonal variability linked to sampling alias in air-sea CO2 fluxes in the Southern Ocean, *Geophys. Res. Lett.*, *42*, 8507–8514, doi:10.1002/2015GL066009.

Naveira Garabato, A. C., K. L. Polzin, B. A. King, K. J. Heywood, and M. Visbeck (2004), Widespread intense turbulent mixing in the Southern Ocean, *Science*, *303*(5655), 210–213, doi:10.1126/science.1090929.

Nicholson, S. A., M. Lévy, J. Llort, S. Swart, and P. M. S. Monteiro (2016), Investigating into the impact of storms on sustaining summer primary productivity in the Sub-Antarctic Ocean, *Geophys. Res. Lett.*, *43*, 9192–9199, doi:10.1002/2016GL069973.

Nikurashin, M., G. K. Vallis, and A. Adcroft (2013), Routes to energy dissipation for geostrophic flows in the Southern Ocean, *Nat. Geosci.*, *6*(1), 48–51, doi:10.1038/ngeo1657.

Orsi, A. H., T. Whitworth III, and W. D. Nowlin Jr. (1995), On the meridional extent and fronts of the Antarctic Circumpolar Current, *Deep Sea Res., Part I*, *42*(5), 641–673.

Paulson, C. A., and J. J. Simpson (1977), Irradiance measurements in the upper ocean, *J. Phys. Oceanogr.*, *7*(6), 952–956, doi:10.1175/1520-0485(1977)007 < 0952:IMITUO>2.0.CO;2.

Price, J. F., R. A. Weller, and R. Pinkel (1986), Diurnal cycling: Observations and models of the upper ocean response to diurnal heating, cooling, and wind mixing, *J. Geophys. Res.*, *91*(C7), 8411–8427, doi:10.1029/JC091iC07p08411.

Rienecker, M. M., et al. (2011), MERRA: NASA's modern-era retrospective analysis for research and applications, *J. Clim.*, *24*(14), 3624–3648, doi:10.1175/JCLI-D-11-00015.1.

Rintoul, S., and T. Trull (2001), Seasonal evolution of the ML in the Subantarctic Zone south of Australia, *J. Geophys. Res.*, *106*(C12), 31,447–31,462.

Rosso, I., A. M. Hogg, P. G. Strutton, A. E. Kiss, R. Matear, A. Klocker, and E. van Sebille (2014), Vertical transport in the ocean due to sub-mesoscale structures: Impacts in the Kerguelen region, *Ocean Modell.*, *80*, 10–23, doi:10.1016/j.ocemod.2014.05.001.

Ruiz, S., A. Pascual, B. Garau, I. Pujol, and J. Tintoré (2009), Vertical motion in the upper ocean from glider and altimetry data, *Geophys. Res. Lett.*, *36*, L14607, doi:10.1029/2009GL038569.

Sallée, J. B., K. G. Speer, and S. R. Rintoul (2010), Zonally asymmetric response of the Southern Ocean mixed-layer depth to the Southern Annular Mode, *Nat. Geosci.*, *3*(4), 273–279, doi:10.1038/ngeo812.

Sallée, J. B., E. Shuckburgh, N. Bruneau, A. J. S. Meijers, T. J. Bracegirdle, and Z. Wang (2013), Assessment of Southern Ocean mixed-layer depths in CMIP5 models: Historical bias and forcing response, *J. Geophys. Res. Oceans*, *118*, 1845–1862, doi:10.1002/jgrc.20157.

Schlitzer, R. (2002), Carbon export fluxes in the Southern Ocean: Results from inverse modeling and comparison with satellite-based estimates, *Deep Sea Res., Part II*, *49*(9–10), 1623–1644, doi:10.1016/S0967-0645(02)00004-8.

Swart, S., et al. (2012), Southern Ocean seasonal cycle experiment 2012: Seasonal scale climate and carbon links, *S. Afr. J. Sci.*, *108*(3/4), 1–3.

Swart, S., S. J. Thomalla, and P. M. S. Monteiro (2015), The seasonal cycle of ML dynamics and phytoplankton biomass in the Sub-Antarctic Zone: A high-resolution glider experiment, *J. Mar. Syst.*, *147*, 103–115, doi:10.1016/j.jmarsys.2014.06.002.

Thomalla, S. J., N. Fauchereau, S. Swart, and P. M. S. Monteiro (2011), Regional scale characteristics of the seasonal cycle of chlorophyll in the Southern Ocean, *Biogeosciences*, *8*(10), 2849–2866, doi:10.5194/bg-8-2849-2011.

Thomalla, S. J., M. Racault, S. Swart, and P. M. S. Monteiro (2015), Investigating the spring bloom initiation and net community production in the Subantarctic Southern Ocean using high-resolution in situ glider data, *ICES J. Mar. Sci.*, *72*(6), 1999–2020, doi:10.1093/icesjms/fsv105.

Thomas, L. N. (2005), Destruction of potential vorticity by winds, *J. Phys. Oceanogr.*, *35*, 2457–2466, doi:10.1175/JPO2830.1.

Thomas, L. N., and C. M. Lee (2005), Intensification of ocean fronts by down-front winds, *J. Phys. Oceanogr.*, *35*(6), 1086–1102.

Thomas, L. N., and R. Ferrari (2008), Friction, frontogenesis, and the stratification of the surface mixed layer, *J. Phys. Oceanogr.*, *38*, 2501–2581, doi:10.1175/2008JPO3797.1.

Thomas, L. N., and J. R. Taylor (2010), Reduction of the usable wind-work on the general circulation by forced symmetric instability, *Geophys. Res. Lett.*, *37*, L18606, doi:10.1029/2010GL044680.

Thompson, A., A. Lazar, C. Buckingham, A. C. Naveira Garabato, G. M. Damerell, and K. J. Heywood (2016), Open-ocean submesoscale motions: A full seasonal cycle of mixed layer instabilities from gliders, *J. Phys. Oceanogr.*, *46*(4), 1285–1307, doi:10.1175/JPO-D-15-0170.1.

Trenberth, K. E. (1991), Storm tracks in the Southern Hemisphere, *J. Atmos. Sci.*, *48*(19), 2159–2178, doi:10.1175/1520-0469(1991)048<2159:STITSH>2.0.CO;2.

Waniek, J. J. (2002), The role of physical forcing in initiation of spring blooms in the north-east Atlantic, *J. Mar. Syst.*, *39*(1), 57–82, doi:10.1016/S0924-7963(02)00248-8.